



Article

Selection Criteria for Biplane Wing Geometries by Means of 2D Wind Tunnel Tests

Ángel Antonio Rodríguez-Sevillano ^{1,*}, Miguel Ángel Barcala-Montejano ¹, Rafael Bardera-Mora ²,
Adelaida García-Magariño García ², María Elena Rodríguez-Rojo ¹, Sara Morales-Serrano ¹
and Jaime Fernández-Antón ¹

- ¹ Escuela Técnica Superior de Ingeniería Aeronáutica y del Espacio (ETSIAE), Universidad Politécnica de Madrid (UPM), 28040 Madrid, Spain; miguel.barcala@upm.es (M.Á.B.-M.); elena.rodriguez.rojo@upm.es (M.E.R.-R.); sara.morales@esa.int (S.M.-S.); jaime.fernandez.anton@alumnos.upm.es (J.F.-A.)
- ² Instituto Nacional de Técnica Aeroespacial (INTA), Torrejón de Ardoz, 28850 Madrid, Spain; barderar@inta.es (R.B.-M.); garciamga@inta.es (A.G.-M.G.)
- * Correspondence: angel.rodriguez.sevillano@upm.es

Abstract: This paper presents a study based on wind tunnel research on biplane configurations. The objective of this research is to establish an experimental basis for relationships between the main geometrical parameters that define a biplane configuration (stagger, decalage, gap, and sweep angle) and the aerodynamic characteristics (C_L , C_D). This experimental study focuses on a 2D approach. This method is the first step towards dealing with the issue, and it allows the variables involved in the tests to be reduced. The biplane configuration has been compared with the monoplane configuration to analyze the viability for implementing the biplane configuration in the field of application for micro air vehicles (MAV). At present, the biplane and other unusual configurations have not been a common design for MAV; however, they do have unlimited future potential. A set of experimental tests were carried out on various biplane configurations at low Reynolds numbers, which allowed the criteria for selecting the best wing configuration to be defined. The results obtained here show that the biplane configuration provides a higher maximum lift coefficient (C_{Lmax}) than the planar wing (monoplane). Furthermore, it has a larger wetted surface than the planar configuration, so the parasitic drag increases for the biplane configuration. This research is focused on a drone flight regime (low Reynolds number), and in this case, the parasitic drag (profile drag) has an important role in the total drag of the airplane. This study considers whether the reduction in the induced drag due to three-dimensional configuration (biplanes, box-wings, and joined-wings) can reduce the total drag or if the increase in the parasitic drag is bigger. Additionally, the increase in lift and the decrease in parasitic drag (profile drag) will be studied to determine if they have a greater influence on the performance of the airplane than the increase in structural weight. Further research is planned to be performed on 3D prototypes, with the selected configurations, and applied to nonconventional wing planforms.

Keywords: biplane configuration; nonplanar wing; low Reynolds regime; aerodynamic behavior; wind tunnel test



Citation: Rodríguez-Sevillano, Á.A.; Barcala-Montejano, M.Á.; Bardera-Mora, R.; García-Magariño García, A.; Rodríguez-Rojo, M.E.; Morales-Serrano, S.; Fernández-Antón, J. Selection Criteria for Biplane Wing Geometries by Means of 2D Wind Tunnel Tests. *Appl. Mech.* **2022**, *3*, 628–648. <https://doi.org/10.3390/applmech3020037>

Received: 8 March 2022

Accepted: 13 May 2022

Published: 16 May 2022

Publisher's Note: MDPI stays neutral with regard to jurisdictional claims in published maps and institutional affiliations.



Copyright: © 2022 by the authors. Licensee MDPI, Basel, Switzerland. This article is an open access article distributed under the terms and conditions of the Creative Commons Attribution (CC BY) license (<https://creativecommons.org/licenses/by/4.0/>).

1. Introduction

Since the beginning of modern aviation in the early twentieth century, much attention has been paid to aircraft with more than one wing surface, and this type of configuration proved to offer a significant reduction in induced drag [1,2]. Despite their suitable characteristics in terms of structural stiffness, over time these configurations required a set of cables and struts and as a result were eventually rejected.

However, they are now included in the conceptual design [3,4] of new configurations—airplanes with nonplanar wings [5], biplanes, box-wings [6,7], joined-wings [8], and

wing tip devices [6–9], among others—for future use in commercial aircraft [10–17] in the design of RPAS (remotely piloted aircraft systems) [18–22]. The nature of RPAS, that is, an air vehicle without a pilot onboard, obviously allows for the possibility of dramatically reducing the size of the vehicles.

The new airplane designs [23,24] deal with changes in the general arrangement of the airplane and the geometry of the wings to enhance the main aerodynamic features (C_{Lmax} , C_{Dmin} , $(C_L/C_D)_{max}$) and the maximum aerodynamic ratios $(C_L^{1/2}/C_D)_{max}$, $(C_L^{3/2}/C_D)_{max}$ related to the main performance of the airplane (E_{max} , R_{max} , x_{max} , etc.).

When the research is focused on RPAS, particularly in micro air vehicles (MAV), it is quite promising to analyze the biplane configuration [17,24,25]. MAVs are limited with stringent constraints [17], and it is necessary to consider the maximum value of the gross area (S) of the wings related to the constraining size (usually, wingspan $-b-$). With the same size, a monoplane configuration leads to a low wing aspect ratio (AR) and therefore, a higher value of the induced drag (D_i). The main effect of biplane wings is to divide D_i by a factor nearly of 2 and, though an increase in parasitic drag (D_O) appears [14].

One of the main ways to improve the aerodynamic behavior of an aircraft is to decrease its drag force (D). According to several authors [9,26], drag coefficient (C_D) can be described in terms of the sum of the minimum profile drag coefficient (C_{Dmin}), the incremental change in profile drag due to lift ($\Delta C_{D_{profile}}$), and the induced drag coefficient (C_{Di}).

The induced drag (D_i) is the drag due to lift (D_{Lift}). D_{Lift} represents roughly half of the total D force when the airplane is flown under flight conditions leading to $(C_L/C_D)_{max}$. During the take-off and landing conditions, the drag force (D) is predominant, but in the cruise condition, the speed is higher than the one corresponding to $(C_L/C_D)_{max}$, so D_O governs the total D force.

One way to improve or reduce D_i is by using nonplanar [27]. A reduction in D_i is achieved in nonplanar wings compared to planar wings of the same span (b) and lift (L) [10]. To compare the amount of D_i reduction, the equivalent monoplane is defined [2,28]. There are numerous nonplanar configurations to consider as candidates to be studied as a way of reducing the D force [29]. Additionally, there are also several methods to improve D_i [30]. If the D force is reduced, it could lead to an increase in R (range) or E (endurance) of the airplane. However, the biplane configuration may produce a theoretical penalty in weight due to additional wings and struts, where the biplane and monoplane configurations are compared for such proposition [8,17].

Our field of interest is the MAV, which are RPAS (drones) of small size, their wingspan being less than 15 cm. This implies dealing with air vehicles flying in the low Reynolds number regime [26,31]. The Reynolds number $Re = \rho Vc/\mu$ is based on flow characteristics, flight conditions, and main vehicle dimensions. Therefore, a flight at low Reynolds numbers implies a relationship between low velocities and small sizes.

A systematic study of the aerodynamics of the biplane and tandem wing at low Reynolds numbers was presented by [32]. The authors of [32] performed a particle image velocimetry (PIV) test to study the flow field, and they also obtained the aerodynamic coefficient for different stagger (s) and gap (G) between two plane wings. However, they did not address sweep angles (Λ) or decalage (δ) between the planes.

The present study is a preliminary investigation based on wind tunnel tests of several biplane configurations including different Λ , δ angles between the planes of the wing. These biplane configurations are simplified prototypes of complex three-dimensional configurations. The objective of this first study is to choose the best configurations according to C_L , C_{Dmin} , $C_{D_{profile}}$ criteria. Based on an appropriate and optimal selection of the wing configuration, the value of D_i would be fixed. Therefore, we have focused this research on the analysis of geometrical parameters of the biplane configuration using a 2D approach. In this first set of tests, we have obtained experimental data about C_L and C_{Dmin} . The main criterion for selecting the best 2D configuration has been the highest value of C_{Lmax} , while

the C_{Dmin} value is discussed as a secondary result. Using the results of the experimental study carried out in this investigation, a relationship between four geometric parameters that has an optimum response to the maximization of the lift (L) is obtained.

First, the description of the parametrical experimental study including the experimental procedure and some specific tests dedicated to ensuring the 2D assumption is presented. Then, the experimental results are shown and discussed. Finally, an experimental design criterion the results are proposed and the main conclusions are summarized.

2. Materials and Methods

2.1. Prototypes Description

Different combinations of geometrical parameters in biplane configurations lead to different aerodynamic behavior. This research carries out a systematic study of the influence of these parameters. A 2D biplane model (a semi prototype) is designed, in which four geometric parameters can be modified: the gap (G), the stagger (s), the angle of decalage (δ), and the sweep angle (Λ), as detailed in [9].

The gap (G) is the vertical distance between the quarter-chord points of each wing (see Figure 1). The angle of decalage (δ) is the relative angle of incidence (θ) between the two wings, according to [9,14].

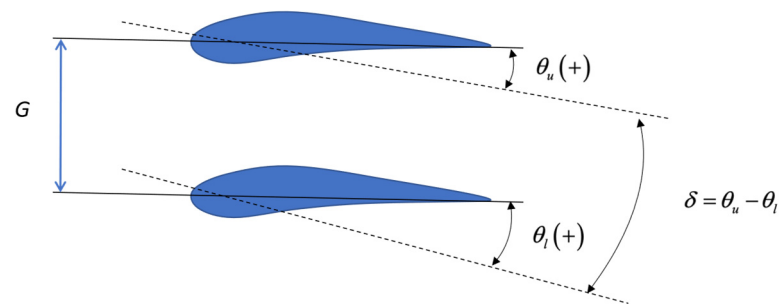


Figure 1. Gap and decalage definition.

The stagger (s) is the longitudinal distance between the leading edge of each wing (see Figure 2). This is positive if the upper wing is in front of the lower wing and negative if it is behind the lower wing, considering in both cases the root sections as the reference. The sweep angle (Λ) is the angle between the line of the quarter chord of the wing and the perpendicular line to the plane symmetry of the airplane.

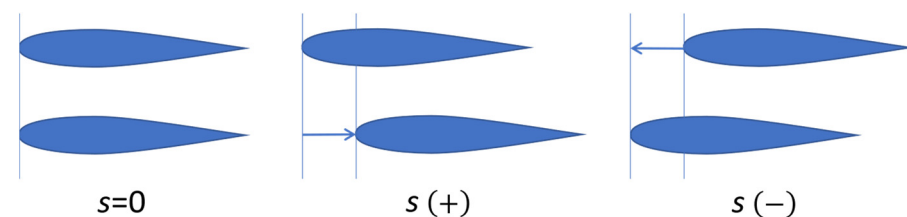


Figure 2. Stagger definition.

Five configurations are considered, each one differing from the rest in terms of the stagger (s) and the sign of Λ , as shown in Figure 3. The distance (s) takes three values: zero and the length of the chord (c), with a negative and positive sign. The value of the sweep angle is $\Lambda = \pm 50^\circ$. The five configurations are distinguished with a pair of capital letters. The letter A represents $\Lambda = 0^\circ$, B represents $\Lambda = -50^\circ$, and C represents $\Lambda = 50^\circ$, according to [9]. The first letter represents the lower wing and the second the upper one.

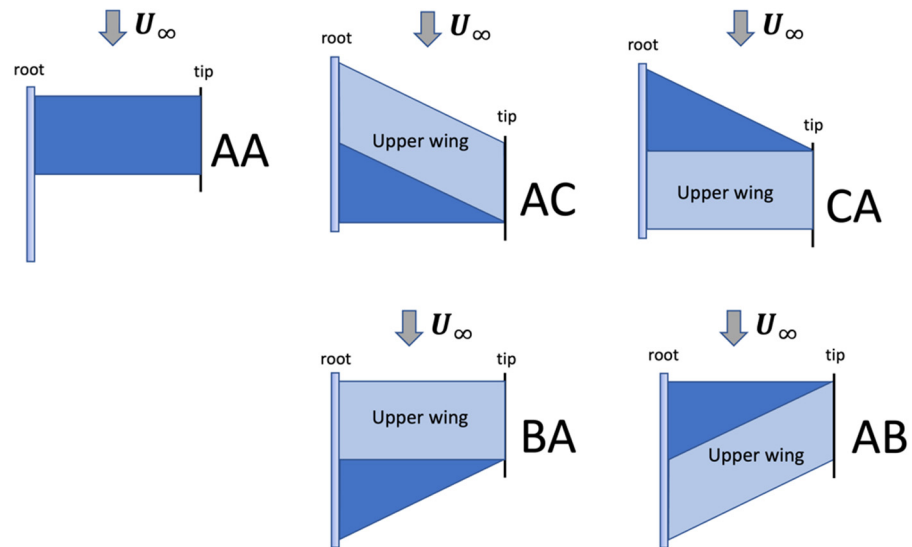


Figure 3. The five different configurations of the prototypes tested. Upper view. Light blue shows the upper wings. In the AA configuration, both wings are superposed.

The variation in G has been represented by two values: one chord length and half a chord length. In the nomenclature of the wing configuration, the specification of G comes after the two capital letters: ‘10’ represents $G = c$ and ‘05’ represents $G = c/2$ (see Figure 4). The fourth modified geometric parameter was δ (the difference between the angle of incidence of both wings). Adding at the end of the model denomination the value of the relative incidence specifies it: $\pm 6, \pm 3, = 0$.

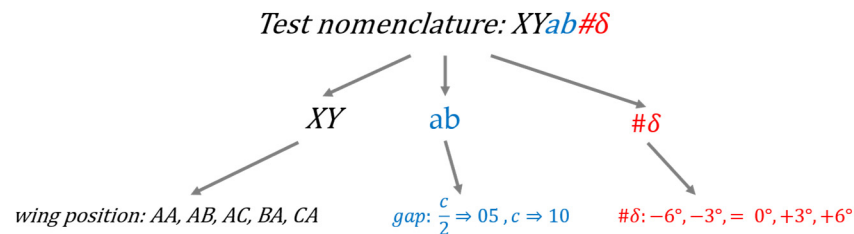


Figure 4. Prototype nomenclature.

For these five configurations, there is a relationship between the sweep angle (Λ) of the upper and lower wings and the value of the stagger (s). These parameters, in the set of tests developed, are not independent. The two profiles at the tip are placed with no horizontal displacement because the two wings are considered joined at the wingtips with an endplate.

The main geometrical parameters of the prototypes are summarized in Table 1.

Table 1. Main geometrical parameters of the prototypes.

Parameters	Values
Wing profile	Eppler E387
Wing chord (c)	160 mm
Wingspan (b)	120 mm
Gap (G)	$c/2, c$
Incidence of upper & lower wings (θ_u, θ_l)	$\pm 3, 0$
Decalage (δ)	$\pm 6, \pm 3, 0$
Stagger (s)	$0, \pm 160$ mm
Sweep angle (Λ)	$0, \pm 50^\circ$
Wing configurations (explained below)	AA, AB, AC, BA, CA

All prototypes were manufactured by a CAD/CAM milling machine and are made up of Necuron material. The selected airfoil is the Eppler E-387, which is appropriate for low Reynolds numbers [33].

The prototype was tested in the wind tunnel as described in the next section. Geometrical parameters were changed systematically during the tests. The design criterion of the prototype is to easily allow for all types of modification of the main geometrical features to be performed during the test program. The model is shown in Figure 5.



Figure 5. Upper and lateral views of the prototype.

The model is connected to the wind tunnel load cell by means of a bar that extends from one of the lateral plates. The plate attached to the load cell represents the fuselage–wing union. Wings with sweep angle (Λ) are moved forward or backward on this plate to achieve the desired configuration. On the other plate, there is no difference in the longitudinal position of the leading edge of the wings.

The general aerodynamic forces were measured in all cases.

2.2. Wind Tunnel Facility

The wind tunnel used for this experiment was an open–circuit, closed–test–section tunnel at the ETSIAE (UPM). The main characteristics of the wind tunnel are shown in Table 2.

Table 2. Characteristics of the wind tunnel.

Characteristics	Description
Speed range	0–30 m/s
Nozzle contraction ratio	9:1
Test section	Square geometry $0.45 \times 0.45 \times 1$ (m)
Power unit	Fan driven by DC Electric Motor 23 kW
Flow uniformity in the test chamber $(U_{max} - U_{min})/\bar{U}$	<1%
Mean turbulence level I_u	<0.5%
Maximum Reynolds Number	$Re_{max} = 6.9 \times 10^5$

The flow uniformity is defined in terms of the ratio of the difference between maximum and minimum values of the speed measured in the test section to the mean speed value. Twenty–five points were considered as representative magnitudes of flow behavior. Additionally, the mean intensity level of the turbulence, according to [34], is defined as the relationship between the standard deviation of the wind speed and the mean speed value:

$$I_u = \frac{\sigma U}{\bar{U}} \quad (1)$$

The models were mounted on one of the tunnel walls. The load cell was attached to the wind tunnel wall, but externally. This allowed one degree of freedom and, therefore, allowed the pitch angle to be changed. This load cell gives three force measurements: aft lift and fore lift and drag. The wind tunnel is provided with a device that allows the wind tunnel speed to be measured by means of the dynamic pressure of the flow (model TT 570CV, DPM).

The aerodynamic forces acting on the model are transmitted to the wind tunnel balance (a three-component electronic balance from PLINT Company), and the output of the balance is connected to a data acquisition system (NI USB-6212 BNC, National Instruments). This hardware converts the analogical signals corresponding to the force measurements to digital signals. These digital signals are processed using a Matlab program that presents and stores the results on a PC. The main characteristics of the wind tunnel balance are presented in Table 3.

Table 3. Characteristics of the balance of the wind tunnel.

Characteristics	Description
Position	Side wall of the test chamber
Degrees of freedom	Three: Lift, Drag, and Pitching Moment
Load cells range	Lift: 100 N Drag: 50 N Moment: 3.1 Nm
Accuracy	Lift: 0.015 N Drag: 0.0076 N Moment: 4.8×10^{-4} Nm
Repeatability (RMS)	Lift: 0.004 Drag: 0.002 Moment: 0.001

The geometric definition of the model matches with our facility, not only with the dimensions of the test chamber of our wind tunnel (to avoid blockage effects), but also with the characteristics of the balance force installed in the tunnel necessary to capture the extremely low drag forces of these wings. Due to these circumstances, this research proposes an alternative method based on a 2D methodology.

2.3. The Two-Dimensional Flow Hypothesis

Before the experiments, the two-dimensional flow hypothesis (2D flow) was evaluated using flow visualization based on tufts. The tufts were attached to the surface of the model and show the direction of the flow. In addition, they also show the stall phenomenon. In a three-dimensional surface, the flow will be not only oriented to the chord direction but also deflected toward the span direction, as can be seen in Figure 6. Therefore, the analysis of the streamline deviation shown with the tufts can validate the two-dimensional flow hypothesis.

The 2D flow evaluation tests were performed in the wind tunnel described previously and are used to obtain drag and lift measurements. The test chamber was replaced for this purpose by a twin methacrylate one (see Figure 7). The configuration used for these tests was the AB configuration (see Figure 8). To carry out the flow visualization test, pictures were taken of the upper surface and lower surface of the upper wing and the lower surface of the lower wing. These tests are performed with a speed flow of $U_\infty = 15$ m/s ($Re = 1.6 \times 10^5$) and $-10^\circ \leq \alpha \leq 10^\circ$ of the angle of attack.

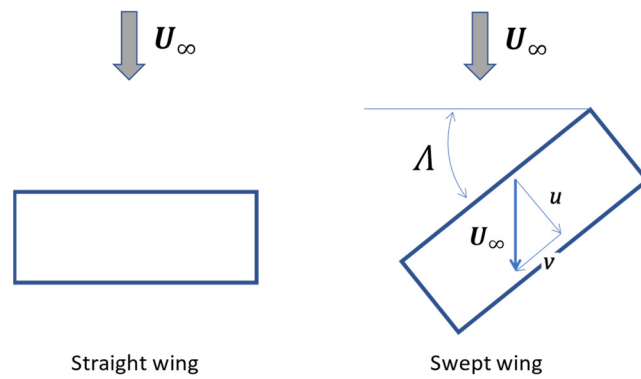


Figure 6. Comparison with the straight wing and the swept wing.

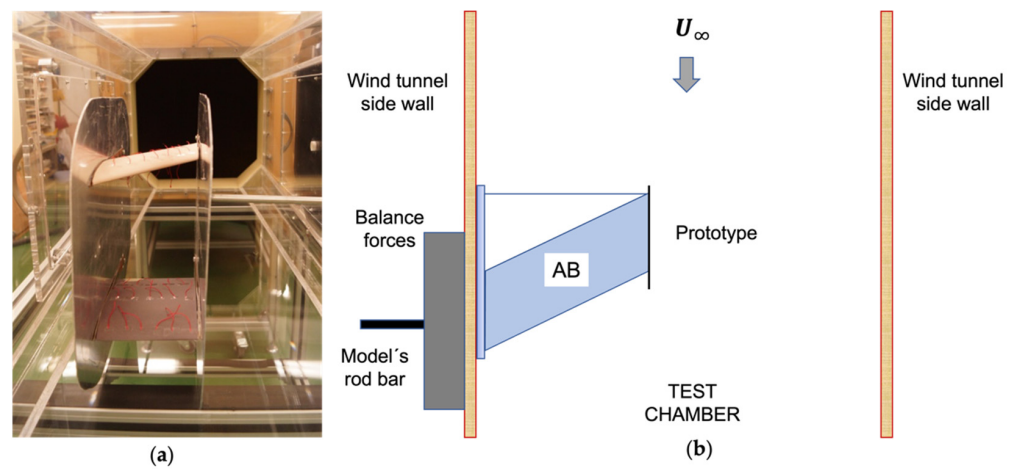


Figure 7. Details of the prototype placed in the wind tunnel. (a) Prototype AB for 2D flow evaluation positioned in the methacrylate test chamber. (b) General view of the wind tunnel's elements.

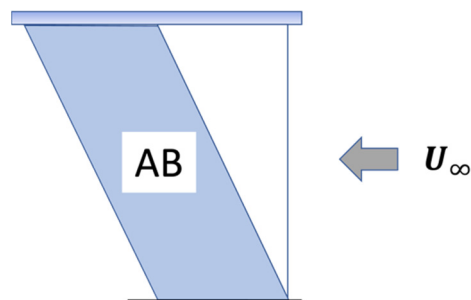


Figure 8. The AB configuration is the one selected to carry out the flow visualization tests; in this figure, the prototype is oriented in the appropriate view according to Figures 8–10.

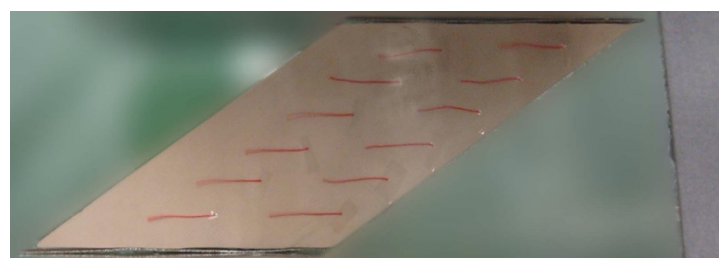


Figure 9. Lower surface of the upper wing.

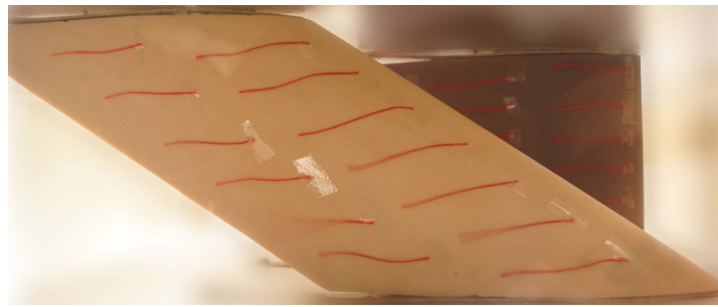


Figure 10. In the foreground, the upper surface of the upper wing. In the background, the upper surface of the lower wing.

Figures 9 and 10 show the lower and upper surfaces of the upper wing, respectively, while Figure 11 shows the upper surface of the lower wing. It shows that for the lower surface of upper wing and the upper surface of the lower wing, two-dimensionality is indeed observed since no deviation of the flow is encountered towards the span direction.



Figure 11. A detailed picture of the upper surface of the lower wing.

In Figure 10 it can be observed that some deviation of the flow has occurred on the upper surface of the upper wing. Figure 12 shows a more detailed analysis of the deviation of the streamlines on the top surface of the upper wing, leading to the conclusion that the streamlines are deflected lightly, although it is not large enough to reject the two-dimensional assumption. Therefore, the two-dimensional flow hypothesis is considered valid in this research, taking into account that the study consists of the definition of several optimum geometries related to aerodynamic criteria.

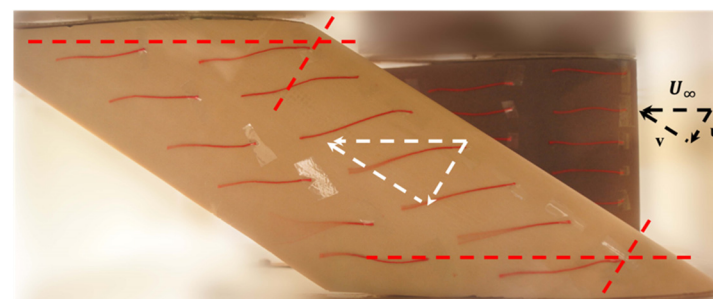


Figure 12. Analysis of the deviation of the streamlines on the upper surface of the upper wing.

2.4. Experimental Test Procedure

For each of these combinations of geometrical parameters, a set of tests was carried out, varying the model (see Figure 13). Rotating a graduated wheel of the load cell caused this variation; the model rod bar attached to the load cell rotates with this wheel, producing

the rotation of the whole model. The interval of variation of the angle of attack was $-15^\circ \leq \alpha \leq 24^\circ$.

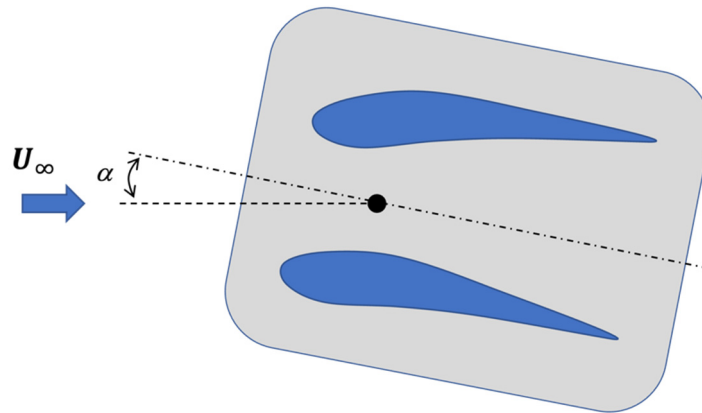


Figure 13. Definition of α the (angle of attack) of the model.

Following this test procedure, fifty runs were carried out. Before any test was performed, the calibration of the balance was completed. The main features of the data acquisition were the following: sampling rate = 500, register duration = 15 s. The air speed for all runs was fixed between 20 m/s and 25 m/s, with the aim of achieving a Reynolds number of 2.1×10^5 . The results obtained were the lift (L) and drag (D) forces. From these forces, the lift and drag coefficients have been calculated.

$$C_L = \frac{L}{\frac{1}{2}\rho U_\infty^2 S}, \quad C_D = \frac{D}{\frac{1}{2}\rho U_\infty^2 S} \tag{2}$$

The wing area is related to each wing configuration as follows:

$$S_{monoplane} = bc, \quad S_{biplane} = 2bc \tag{3}$$

The relationship between lift coefficients (C_L) will be the same as the relationship between lift forces in the wind tunnel tests.

3. Results

The variables to be studied were the maximum lift coefficient (C_{Lmax}), the minimum profile drag coefficient (C_{Dmin}), and the lift slope ($C_{L\alpha}$). C_{Lmax} is related to the minimum speed required for flight (stall speed), in level conditions, for a fixed altitude, weight, and wing configuration. Low values of C_{Dmin} imply less energy than the wing configuration loses in its interaction with the flow. The low loss of energy allows for a greater time (E , endurance) and distance (R , range) of the aircraft provided with this wing configuration. $C_{L\alpha}$ shows that the lower the value, the higher α necessary for a fixed flight condition of C_L . Finally, high values of $(C_L/C_D)_{max}$ lead to more efficient flights. In a jet aircraft, the maximum value of this ratio corresponds to E_{max} ; in a propeller aircraft, the maximum corresponds to R_{max} . Additionally, C_{L0} and $\alpha_{C_{Dmin}}$ are also studied.

A complete set of tests were carried out that vary the following parameters: wing configuration (either AA, AB, AC, BA, or CA), G (either half of the chord or the chord), and δ (either -6° , -3° , 0 , $+3^\circ$ or $+6^\circ$). To accomplish these, an ensemble of tests was made with a monoplane prototype. The monoplane is used as a reference for each parameter.

Finally, it should be mentioned that the drag force of the strut is $D_{strut} = 0.761 \text{ N}$ and is included in all the results of the drag forces of each prototype.

Figure 14 plot C_{Lmax} versus δ (for each gap $-G-$ tested) for the five wing configurations AA, AB, BA, AC, and CA. Firstly, it is noted that C_{Lmax} increases with the gap (the symbols filled in colors corresponding to a gap of one chord are above the symbols filled in white corresponding to a half-chord gap). This is consistent with the explanation provided

by [25]: as the G-gap is reduced, there is a strong interference between the two wings, and a severe reduction in C_L is produced. On the other hand, it can be observed in the same figure that for the wing configurations AA, AB, and BA, where the swept wing was $\Lambda \leq 0$, there is a relationship between δ and C_{Lmax} that depends on the wing configuration. For the wing configurations AA and BA, C_{Lmax} decreases as δ increases; these wings configurations have values of s —stagger—above or equal to zero. On the contrary, for the AB wing configuration, where the $s < 0$ (stagger negative), C_{Lmax} increases as δ increases. For those configurations of wings where the swept angle of the wings was $\Lambda \geq 0$ (configuration AC and CA), C_{Lmax} seems to remain constant with δ . Now, the ten highest values of C_{Lmax} are presented in Figure 15. These results are presented in terms of percentage with respect to the monoplane C_{Lmax} value (the higher the maximum lift, the smaller the percentage difference). Eight out of the ten values correspond to the AC configuration of the wing. Therefore, the best results in terms of C_{Lmax} were achieved in the AC configuration.

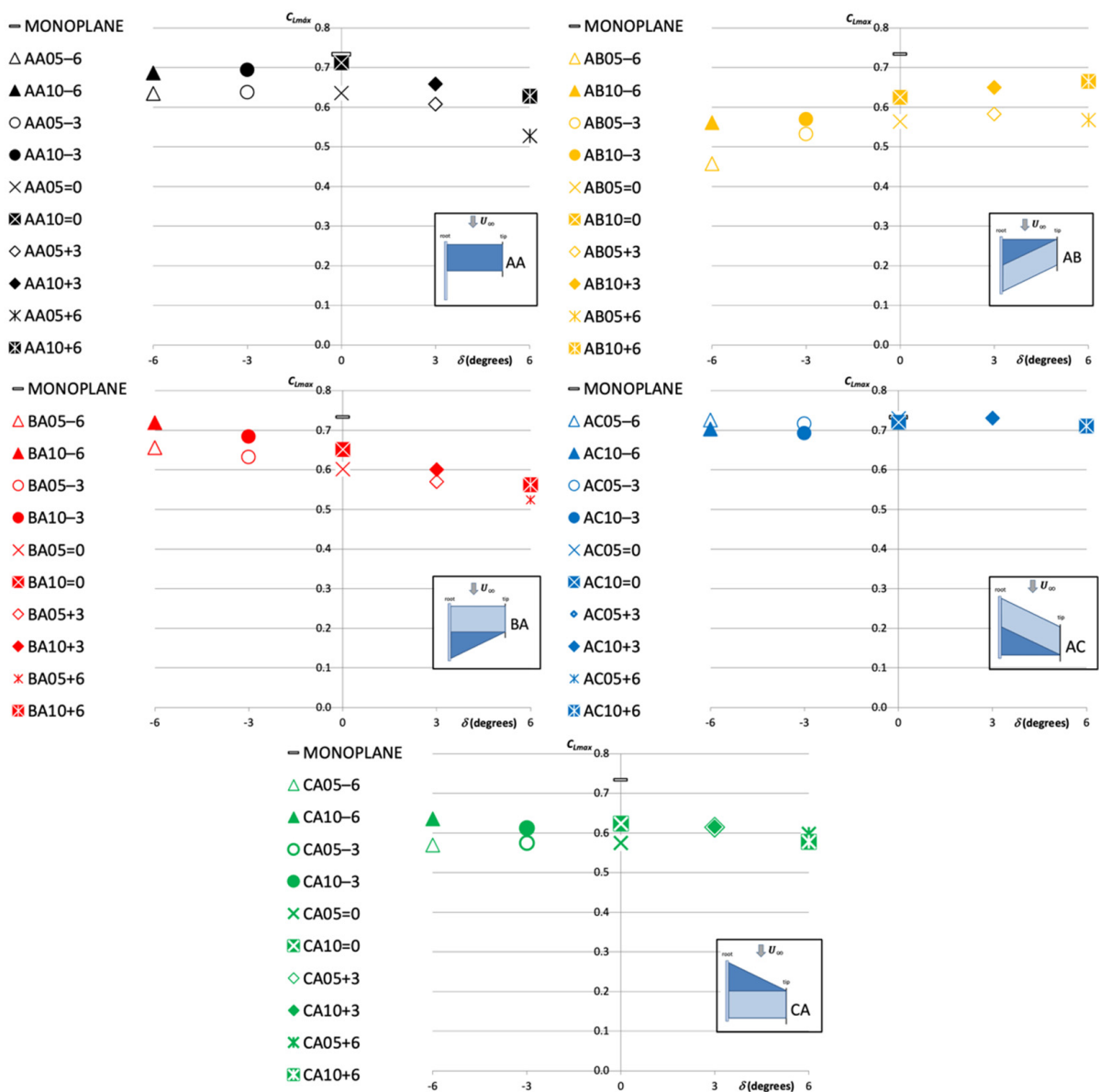


Figure 14. C_{Lmax} vs. δ for AA, AB, BA, AC, and CA configurations.

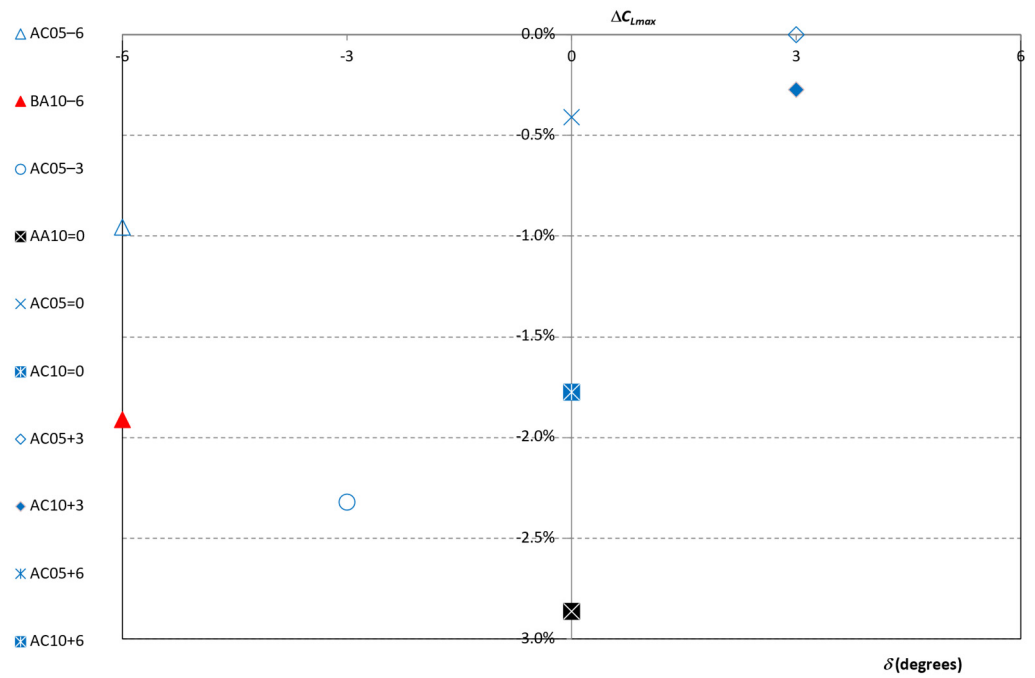


Figure 15. Top ten configurations according to the highest C_{Lmax} criteria in terms of percentage with respect to the monoplane C_{Lmax} value.

Table 4 shows the lift slope $C_{L\alpha}$ for all the tests conducted. It seems to remain nearly constant for all configurations.

Table 4. Lift slope for each configuration.

AA05-6 0.032	AA10-6 0.036	AB05-6 0.032	AB10-6 0.034	AC05-6 0.032	AC10-6 0.032	BA05-6 0.032	BA10-6 0.033	CA05-6 0.031	CA10-6 0.031	AA05-6 0.032	AA10-6 0.036
AA05-3 0.033	AA10-3 0.037	AB05-3 0.035	AB10-3 0.034	AC05-3 0.031	AC10-3 0.033	BA05-3 0.032	BA10-3 0.034	CA05-3 0.034	CA10-3 0.032	AA05-3 0.033	AA10-3 0.037
AA05=0 0.032	AA10=0 0.036	AB05=0 0.035	AB10=0 0.034	AC05=0 0.032	AC10=0 0.034	BA05=0 0.031	BA10=0 0.034	CA05=0 0.031	CA10=0 0.033	AA05=0 0.032	AA10=0 0.036
AA05+3 0.027	AA10+3 0.034	AB05+3 0.034	AB10+3 0.035	AC05+3 0.034	AC10+3 0.033	BA05+3 0.031	BA10+3 0.032	CA05+3 0.030	CA10+3 0.032	AA05+3 0.027	AA10+3 0.034
AA05+6 0.026	AA10+6 0.033	AB05+6 0.032	AB10+6 0.034	AC05+6 0.031	AC10+6 0.031	BA05+6 0.031	BA10+6 0.032	CA05+6 0.032	CA10+6 0.033	AA05+6 0.026	AA10+6 0.033
AA05-6 0.032	AA10-6 0.036	AB05-6 0.032	AB10-6 0.034	AC05-6 0.032	AC10-6 0.032	BA05-6 0.032	BA10-6 0.033	CA05-6 0.031	CA10-6 0.031	AA05-6 0.032	AA10-6 0.036

Figure 16 plots C_{Lo} values versus δ angle (for each gap tested) for the five wing configurations AA, AB, BA, AC, and CA. First, a linear relationship between C_{Lo} and δ is evidenced in most of the cases. Then, it can be observed that for those wing configurations where $s < 0$ (configuration AB and CA), the increase in C_{Lo} seems to be greater. However, overall higher values of the C_{Lo} are observed for those wing configurations with $s \geq 0$ (configurations AA, BA and AC). The top ten values are presented in Figure 17, which are the highest values corresponding to the tests AC05+6, BA10+6, and AA10+6. These results are also presented in terms of percentage with respect to the C_{Lo} value for the monoplane configuration.

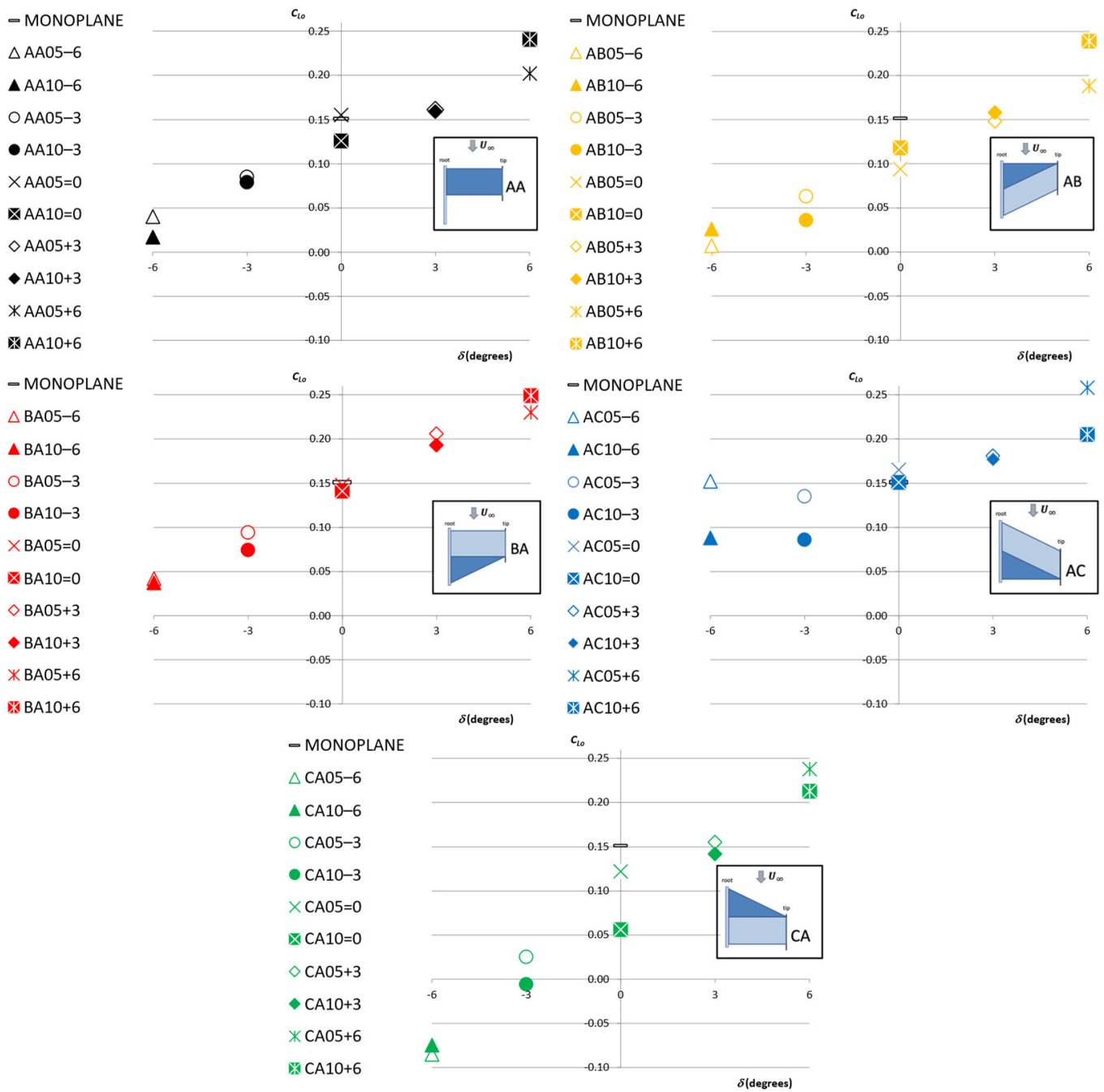


Figure 16. $C_{L\alpha}$ lift coefficient vs. δ for AA, AB, BA, AC, and CA configurations.

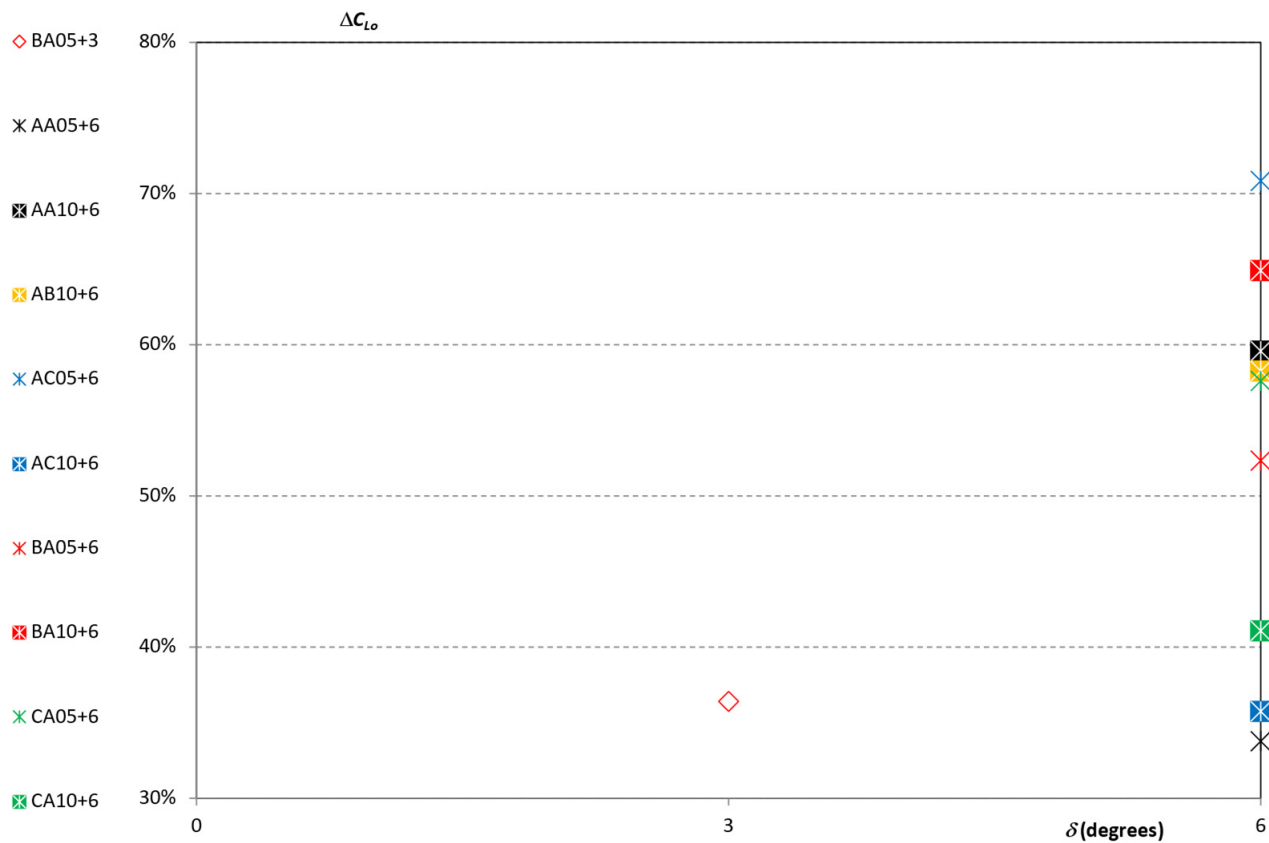


Figure 17. Top ten configurations according to higher C_{L_o} values in terms of percentage with respect to C_{L_o} for the monoplane configuration.

If the curve of C_D versus α is analyzed, the $C_{D_{min}}$ value can be obtained for a specific angle of attack $\alpha_{C_{D_{min}}}$. Figure 18 plots $C_{D_{min}}$ versus δ (for each G tested) for the five wing configurations AA, AB, BA, AC, and CA. It can be observed that the $C_{D_{min}}$ values are usually obtained for $\delta = 0$ angle.

The lowest ten values of $C_{D_{min}}$ are shown in Figure 19 in terms of percentages with respect to the $C_{D_{min}}$ for the monoplane configuration, while the $\alpha_{C_{D_{min}}}$ for each of the cases is shown in Figure 20. As the δ angle increases, the value of the $\alpha_{C_{D_{min}}}$ decreases. The lowest $C_{D_{min}}$ correspond to the AC configuration of the prototype.

For all the three criteria, $C_{L_{max}}$, C_{L_o} , and $\alpha_{C_{D_{min}}}$, the best wing configuration is AC ($s = c$ and $\Lambda \geq 0$). Additionally, the minimum values of $\alpha_{C_{D_{min}}}$ are found for $\delta \geq 0$. Therefore, in Figures 21–23, the results for AC05+3, AC10+3, AC05+6, and AC10+6 are shown. Figure 21 shows C_L versus α , while Figure 22 shows C_D versus α . Finally, Figure 23 shows the polar plot.

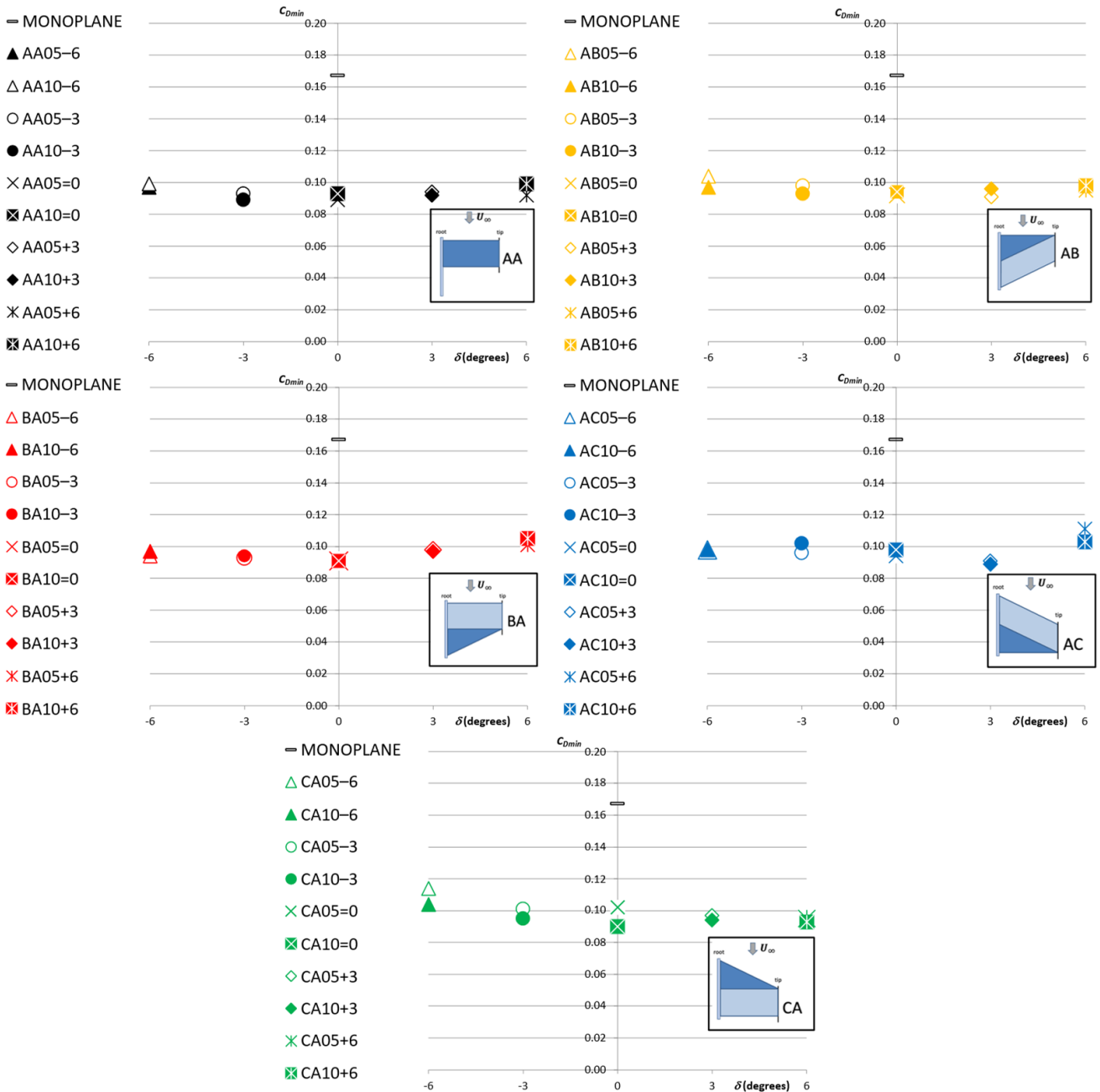


Figure 18. C_{Dmin} vs. δ for AA, AB, BA, AC, and CA configurations.

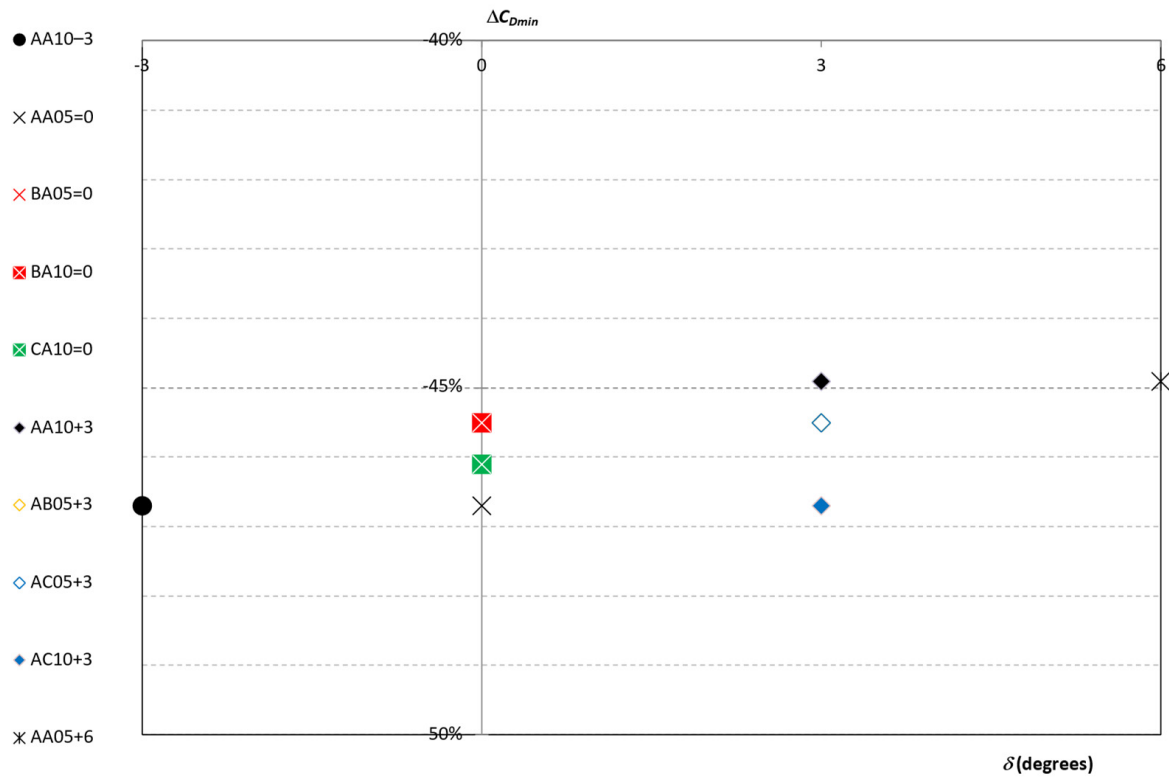


Figure 19. Top ten configurations according to lower C_{Dmin} criteria in terms of percentage with respect to the C_{Dmin} for the monoplane configuration.

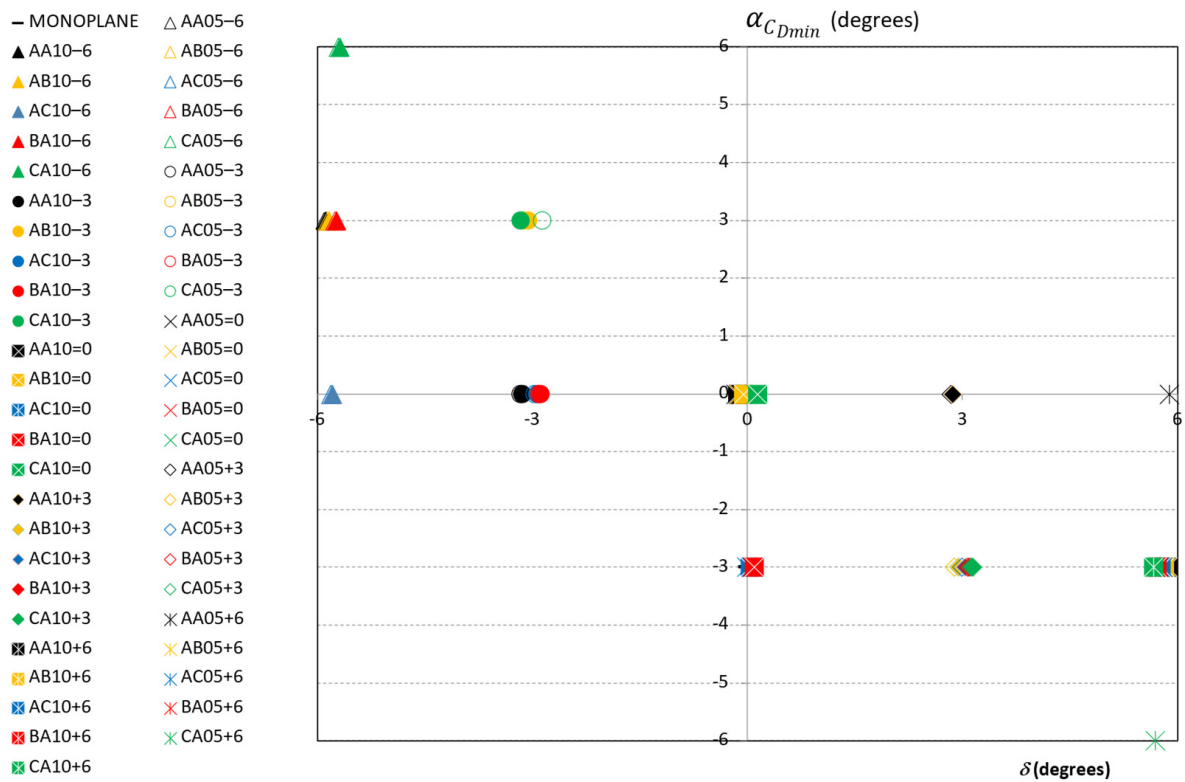


Figure 20. Values of α_{CDmin} for all the configurations.

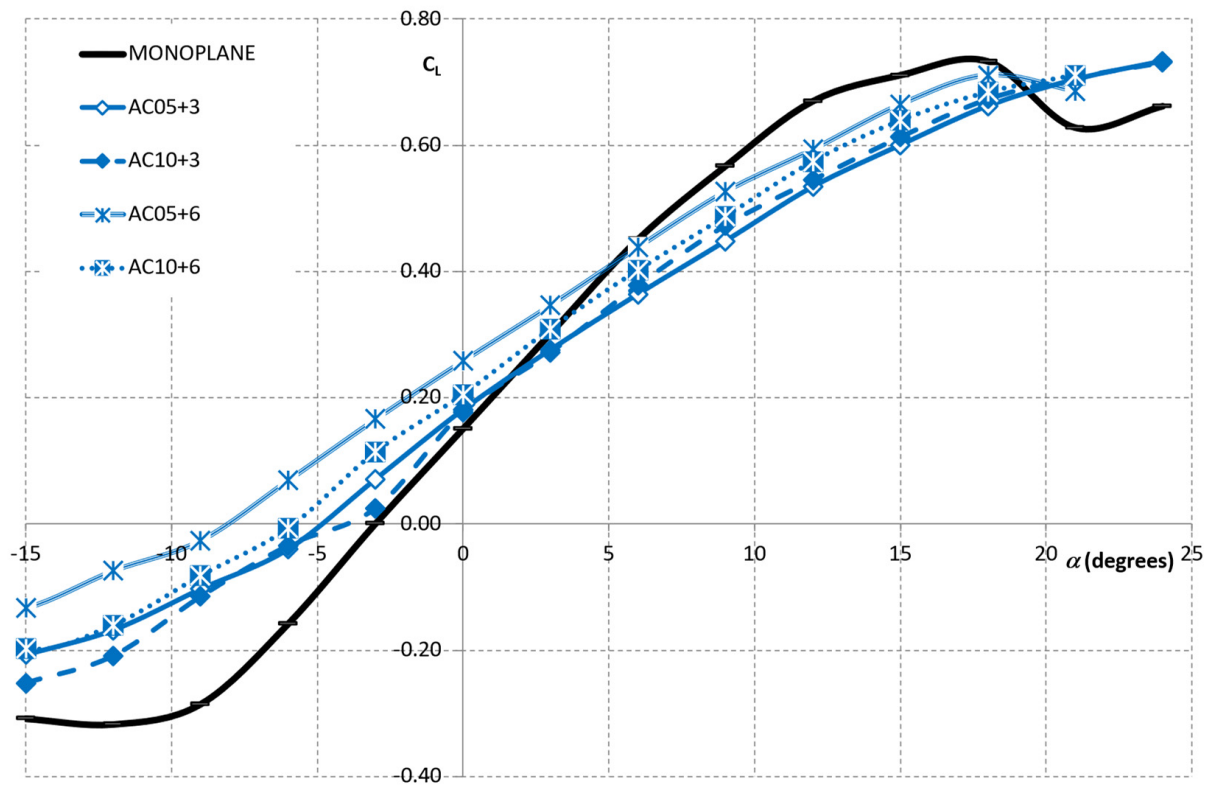


Figure 21. Variation in C_L as a function of α for AC05+3, AC10+3, AC05+6, AC10+6, and monoplane configurations.

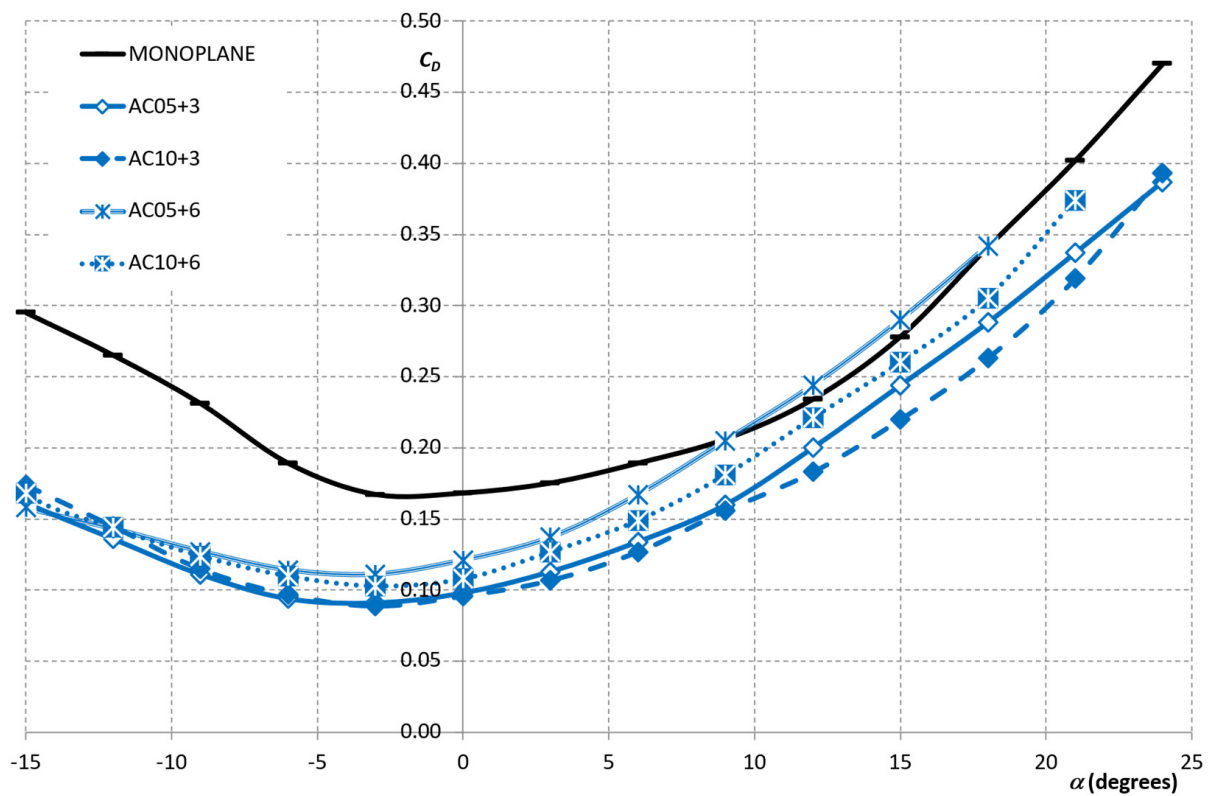


Figure 22. Variation of C_D as a function of α for AC05+3, AC10+3, AC05+6, AC10+6, and monoplane configurations.

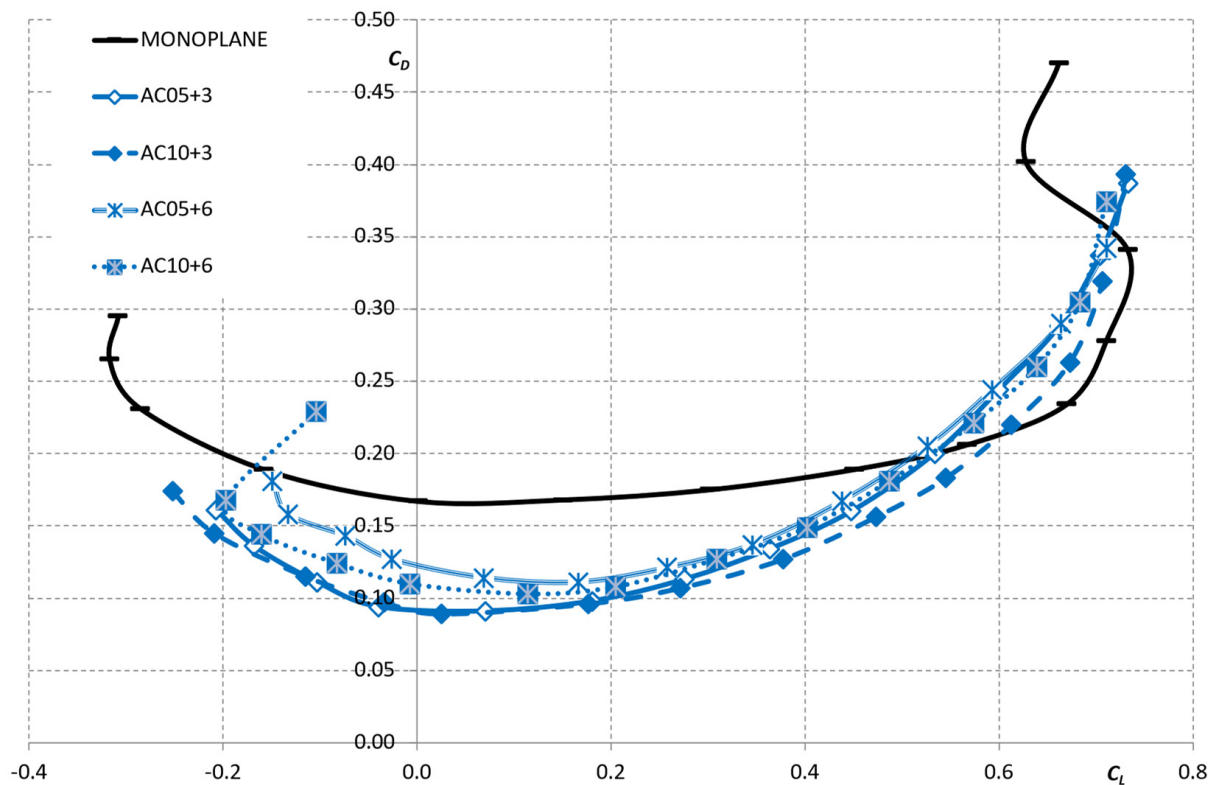


Figure 23. Variation in C_D as a function of C_L (polar curve) for AC05+3, AC10+3, AC05+6, AC10+6, and monoplane configurations.

In the graphs above, the monoplane values are included as a reference. It should be noted that the monoplane configuration achieves higher values of C_{Lmax} and higher values of C_D as a function of α . Owing to the origin of wind tunnel aerodynamic forces, in the monoplane prototype (model with only one wing) $S_{monoplane}$ is half its value as in the biplane prototypes, $S_{biplane}$. Therefore, the aerodynamic forces of the monoplane, which are multiplied by the wing area, would be half of the aerodynamic forces of the biplane for the same aerodynamic coefficient. In the case of the lift, the C_{Lmax} is greater in the monoplane configuration, and the total lift (L) is greater in the biplane configurations. In the case of drag, however, the C_D is smaller in the biplane configuration (almost half of the monoplane one), the total drag (D) in the biplane configuration is close to the monoplane configuration.

4. Discussion

The main objective of this work is to establish the criteria to select the main geometric parameters of the wings of the biplane aircraft according to the criteria for aerodynamic coefficients. The results in the aerodynamic wind tunnel are compared to those of the monoplane wing. This monoplane wing is just one wing of the prototype. It should be noted that the biplane configurations in this research have the double wing area compared with the monoplane wing (one wing); that is, with the same value of C_L , the biplane wing will generate nearly double the value of L . However, in the present study, the objective is not to find a biplane configuration that improves certain aerodynamic characteristics of the monoplane wing but to choose the appropriate configuration (based on an aerodynamic criterion ready to define) of the biplane wing.

This bidimensional experimental study is the first basic part of the complete aerodynamic analysis of the MAV. Analysis of the vehicle aerodynamic and performance could set the main objective as follows: the reduction in drag (D) at close speeds to the take-off and landing conditions or, the reduction in drag (D) in cruise condition or, the increase in lift (L) in certain condition (take off, landing, cruise).

The lift (L) should at least compensate for weight (W) under the trim condition, thus equilibrating the MAV. The biplane structure, generally, may lead to a higher airplane weight, which would be a penalty. The weight (W) increase should be analyzed in the final configuration. On the other hand, the biplane configuration reduces the wing span (b), which results in the beneficial results of a reduced-size airplane, despite the weight penalization. The L force on the prototypes tested in the wind tunnel can be expressed as follows:

$$L_{prototype} = \frac{1}{2} \rho_{test} U_{test}^2 S_{prototype} C_{L_{prototype}} \tag{4}$$

where ρ stands for density, U for velocity, S for wing surface, and C_L for lift coefficient. It is interesting to compare the prototypes by defining a relationship between the lift of the prototypes tested. For each two prototypes, named 'prototype i ' and 'prototype j ':

$$prototype\ i : L_i = q_i S_i C_{L_i} \quad prototype\ j : L_j = q_j S_j C_{L_j} \tag{5}$$

where $q = \frac{1}{2} \rho_{test} U_{test}^2$ stands for dynamic pressure in the wind tunnel test.

The relation between lifts is defined as follows:

$$L_{ij}(\%) = \frac{L_i}{L_j} = \frac{q_i S_i C_{L_i}}{q_j S_j C_{L_j}} = q_{ij} S_{ij} C_{L_{ij}} \tag{6}$$

According to [4,15,35,36] and based on the experience of the authors with the design of the MAV, it is possible to make a rough estimation of the weight of the wing (close to 0.25 kg or lighter). An interesting proposal is included in [17]. Taking into account the cruising flight condition, it is possible to define several design criteria (see Table 5). In this case, we describe two of these criteria, where the subscript ' m ' stands for monoplane configuration and ' b ' stands for the biplane configuration:

Table 5. Design criteria.

Case	Test Conditions	Design Criteria	$C_{L_{mb}}$	q_{mb}	Flight Conditions	Conclusions
1	$S_b = 2S_m$	$L_{mb} = 1$	$C_{L_{mb}} > 1$	$q_{mb} = \frac{2}{C_{L_{mb}}} > 1b\ usions$	$q_m > q_b$	$\Downarrow V_{stall_b}$
2	$S_b = 2S_m$	$L_{mb} > 1$	$C_{L_{mb}} = 1$	$q_{mb} = 2L_{mb}b\ usions$	$L_m > L_b$	$\Downarrow W_b\ (cruise)$

In this first step of the research, we only analyzed the best biplane configuration. The conclusion is clear: the biplane configuration generates more lift (L) [14]. This is obvious: when all the parameters are kept constant, the higher the S , and the more L . Furthermore, it is necessary to consider the increase in W due to S [17]. Other considerations have been put to one side such as the D force, α for level flight condition, $b_{maximum}$, weight distribution, control surfaces, etc. [14], confirming that a biplane wing will have more C_L/C_D than the monoplane wing (meanwhile, S is not the same). However, according to [24], the biplane configuration inevitably means an increase in weight and, at the same time, a notable increase in parasitic drag.

These conclusions are close to the main objective of our research. The objective of this research was to carry out a comparison between several biplane and conventional wing configurations while achieving a criterion for an appropriate selection process for future 3D model tests. The testing of these 3D models is oriented to a final optimization of the MAV design. From the conclusions explained above, the AC configuration was established as the most appropriate, considering mainly the aerodynamic criteria of $C_{L_{max}}$, but also $C_{D_{min}}$ and C_{L_0} . Our results are in accordance with [14]; that is, $s > 0$ increases $C_{L_{max}}$ but does not degrade the C_L/C_D relationship. With the configuration selected, the gap (G) plays a vital role in the flow interference between the wings [25].

5. Conclusions

A parametric study was carried out on the biplane wings configuration that varied δ , s , G , and Λ . The influence of these parameters on the aerodynamic coefficient was studied. The main conclusions are as follows:

- C_{Lmax} increases with G .
- For those wing configurations where $\Lambda \leq 0$, there is a relationship between δ and C_{Lmax} that depends on the wing configuration. For those configurations where $s \geq 0$, C_{Lmax} decreases as δ increases. On the contrary, for the wing configuration where $s < 0$, the C_{Lmax} increases as δ increases.
- For those wing configurations where the wing's swept angle was $\Lambda \geq 0$, C_{Lmax} seems to remain constant with δ .
- $C_{L\alpha}$ seems to remain nearly constant.
- A linear relationship between the C_{L0} and δ is evidenced for most of the cases. For those wing configurations where $s < 0$, the increase in C_{L0} seems to be greater. However, the overall higher values of C_{L0} are observed for those wing configurations with $s \geq 0$.
- The minimum value of C_{Dmin} are usually obtained for $\delta = 0$.
- As δ increases, the value of $\alpha_{C_{Dmin}}$ decreases.

Based on the main conclusions presented above, there are enough criteria to establish appropriate configurations for further research into 3D prototypes. These future tests should be developed with prototypes with a higher wing aspect ratio ($AR \geq 4$) to be compared with the results presented in this document. Finally, when considering the three main aerodynamic features, the AC configuration was chosen as the most aerodynamically appropriate.

Author Contributions: Conceptualization, Á.A.R.-S., M.Á.B.-M., R.B.-M.; data curation, Á.A.R.-S., R.B.-M., M.E.R.-R., S.M.-S.; formal analysis, Á.A.R.-S., M.Á.B.-M., R.B.-M., A.G.-M.G.; funding acquisition, Á.A.R.-S., M.Á.B.-M., R.B.-M.; investigation, Á.A.R.-S., M.Á.B.-M., R.B.-M., M.E.R.-R., S.M.-S., A.G.-M.G., J.F.-A.; methodology, Á.A.R.-S., M.Á.B.-M., R.B.-M.; project administration, Á.A.R.-S., M.Á.B.-M.; resources, Á.A.R.-S., M.Á.B.-M.; software, M.E.R.-R., S.M.-S.; supervision, M.Á.B.-M.; validation, Á.A.R.-S., M.Á.B.-M., R.B.-M., A.G.-M.G.; visualization, Á.A.R.-S., R.B.-M., A.G.-M.G., J.F.-A.; writing—original draft preparation, Á.A.R.-S., R.B.-M., M.E.R.-R., S.M.-S., A.G.-M.G., J.F.-A.; writing—review and editing, Á.A.R.-S., R.B.-M., A.G.-M.G., J.F.-A. All authors have read and agreed to the published version of the manuscript.

Funding: This research received no external funding.

Institutional Review Board Statement: Not applicable.

Informed Consent Statement: Not applicable.

Data Availability Statement: Not applicable.

Conflicts of Interest: The authors declare no conflict of interest.

Abbreviations

The following abbreviations are used in this manuscript:

MAV	Micro Air Vehicles
PIV	Particle Image Velocimetry
RMS	Root mean square
RPAS	Remotely Piloted Aircraft System
UAV	Unmanned Air Vehicle

The following nomenclature is used in this manuscript:

AR	Wing Aspect Ratio $AR = \frac{b^2}{S}$
b	Wingspan
c	Wing chord length

C_L	Lift coefficient $C_L = \frac{L}{\frac{1}{2}\rho U_\infty^2 S}$
$C_{L\alpha}$	Lift slope coefficient
C_{L0}	Lift coefficient for zero angle of attack
C_{Lmax}	Maximum lift coefficient
C_D	Drag coefficient $C_D = \frac{D}{\frac{1}{2}\rho U_\infty^2 S}$
C_{DO}	Parasitic drag coefficient
C_{Di}	Induced drag coefficient; drag due to lift
C_{Dmin}	Minimum profile drag coefficient
C_L/C_D	Lift-to-drag ratio
D	Drag
D_i	Induced drag
D_o	Parasitic drag
D_{Lift}	Drag due to lift
E	Endurance. The time that an aircraft can fly between takeoff and landing based on several flight conditions.
E_{max}	Maximum endurance
G	Gap
I_u	Mean turbulence intensity level $I_u = \frac{\sigma_u}{U}$.
L	Lift
$q = \frac{1}{2}\rho U_{test}^2$	Dynamic pressure $q = \frac{1}{2}\rho U_\infty^2$
R	Range. Distance an aircraft can fly between takeoff and landing based on several flight conditions.
R_{max}	Maximum range
Re	Reynolds number $Re = \frac{\rho U c}{\mu}$
S	Wing gross area
$S_{monoplane}$	Wing area in the monoplane configuration $S_{monoplane} = bc$
$S_{biplane}$	Wing area in the biplane configuration $S_{biplane} = 2bc$
s	Stagger
\bar{U}	Mean value of air speed
U_{max}	Maximum value of air speed on wind tunnel test section
U_{min}	Minimum value of air speed on wind tunnel test section
U_∞	Freestream velocity
x_{max}	Maximum horizontal distance in gliding flight. Distance that an aircraft can glide in a gliding flight based on several flight conditions.
W	Weight
α	Angle of attack
$\alpha_{C_{Dmin}}$	Angle of attack for the minimum drag coefficient
δ	Angle of decalage $\delta = \theta_u - \theta_l$
$\Delta C_{D_{profile}}$	Increment in the profile drag coefficient due to lift
θ	Angle of incidence of each profile
ρ	Air density
μ	Dynamic viscosity of air
σ_U	Standard deviation of U
Λ	Sweep angle

References

1. Munk, M.M. *The Minimum Induced Drag of Airfoils*; NACA TR 121; US Government Printing Office: Washington, DC, USA, 1923.
2. Prandtl, L. *Induced Drag of Multiplanes*; NACA TN 182; US Government Printing Office: Washington, DC, USA, 1924.
3. Jemitola, P.O.; Fielding, J.P. Box Wing Aircraft Conceptual Design. In Proceedings of the 28th Congress of the International Council of the Aeronautical Sciences, Brisbane, Australia, 23–28 September 2012; pp. 1–10. Available online: http://www.icas.org/ICAS_ARCHIVE/ICAS2012/PAPERS/213.PDF (accessed on 7 March 2022).
4. Jemitola, P.O.; Monterzino, G.; Fielding, J. Wing mass estimation algorithm for medium range box wing aircraft. *Aeronaut. J.* **2013**, *117*, 329–340. [[CrossRef](#)]

5. Kroo, I. Nonplanar wing concepts for increased aircraft efficiency. *VKI Lect. Ser. Innov. Config. Adv. Concepts Futur. Civ. Aircr.* **2005**, *1*, 6–10.
6. Khan, F.; Krammer, P.; Scholz, D. Preliminary Aerodynamic Investigation of Box-Wing Configurations Using Low Fidelity Codes. *Dtsch. Luft- und Raumfahrtkongress Doc.* **2010**, *161308*, 313–327.
7. Barcala Montejano, M.A.; Cuerno Rejado, C.; Gandia Agüera, F.; Rodriguez Sevillano, A.; Del Giudice, S. Experimental investigation on box-wing configuration for UAS. In Proceedings of the Unmanned Air Vehicle Systems, Bristol, UK, 11–12 April 2011.
8. Wolkovitch, J. The joined wing—An overview. *J. Aircr.* **1986**, *23*, 161–178. [[CrossRef](#)]
9. Gall, P.D.; Smith, H.C. Aerodynamic characteristics of biplanes with winglets. *J. Aircr.* **1987**, *24*, 518–522. [[CrossRef](#)]
10. Kroo, I. Drag due to lift: Concepts for prediction and reduction. *Annu. Rev. Fluid Mech.* **2001**, *33*, 587–617. [[CrossRef](#)]
11. Kroo, I. Innovations in aeronautics. In Proceedings of the 42nd AIAA Aerospace Sciences Meeting and Exhibit, Reno, NV, USA, 5–8 January 2004; p. 1.
12. Torenbeek, E. Blended-wing-body and all wing airliners. In Proceedings of the 8th European Workshop on Aircraft Design Education, Samara, Russia, 29 May–2 June 2007.
13. Abbas, A.; de Vicente, J.; Valero, E. Aerodynamic technologies to improve aircraft performance. *Aerosp. Sci. Technol.* **2013**, *28*, 100–132. [[CrossRef](#)]
14. Moschetta, J.-M.; Thipyopas, C. Optimization of a biplane micro air vehicle. In Proceedings of the 23rd AIAA Applied Aerodynamics Conference, Toronto, ON, Canada, 6–9 June 2005; p. 4613.
15. Shkarayev, S.V.; Ifju, P.G.; Kellogg, J.C.; Mueller, T.J. *Introduction to the Design of Fixed-Wing Micro Air Vehicles Including Three Case Studies*; American Institute of Aeronautics and Astronautics: Reston, VA, USA, 2007.
16. Reg, A. *Unmanned Aircraft Systems: UAVS Design, Development and Deployment*; John Wiley & Sons: Hoboken, NJ, USA, 2011.
17. Thipyopas, C.; Moschetta, J.-M. A fixed-wing biplane MAV for low speed missions. *Int. J. Micro Air Veh.* **2009**, *1*, 13–33. [[CrossRef](#)]
18. Phillips, P.; Hrishikeshavan, V.; Rand, O.; Chopra, I. Design and development of a scaled quadrotor biplane with variable pitch proprotors for rapid payload delivery. In Proceedings of the American Helicopter Society 72nd Annual Forum, West Palm Beach, FL, USA, 17–19 May 2016; pp. 17–19.
19. Ryseck, P.; Yeo, D.; Hrishikeshavan, V.; Chopra, I. Aerodynamic and mechanical design of a morphing winglet for a quadrotor biplane tail-sitter. In Proceedings of the Vertical Flight Society 8th Autonomous VTOL Symposium, virtual, 26–28 January 2019; pp. 29–31.
20. Bogdanowicz, C.; Hrishikeshavan, V.; Chopra, I. Development of a quad-rotor biplane MAV with enhanced roll control authority in fixed wing mode. In Proceedings of the American Helicopter Society, 71st Annual Forum, Virginia Beach, VA, USA, 5–7 May 2015.
21. Strom, E. Performance and Sizing Tool for Quadrotor Biplane Tailsitter UAS. Ph.D. Thesis, University of Maryland, College Park, MD, USA, 2017.
22. Deng, S.; Xiao, T.; van Oudheusden, B.; Bijl, H. Numerical investigation on the propulsive performance of biplane counter-flapping wings. *Int. J. Micro Air Veh.* **2015**, *7*, 431–439. [[CrossRef](#)]
23. McMasters, J.H.; Kroo, I.M. Advanced configurations for very large transport airplanes. *Aircr. Des.* **1998**, *1*, 217–242. [[CrossRef](#)]
24. Moschetta, J.-M.; Thipyopas, C. Aerodynamic Performance of a Biplane Micro Air Vehicle. *J. Aircr.* **2007**, *44*, 291–299. [[CrossRef](#)]
25. Maqsood, A.; Hiong, T. Go Parametric studies and performance analysis of a biplane micro air vehicle. *Int. J. Aeronaut. Space Sci.* **2013**, *14*, 229–236. [[CrossRef](#)]
26. Spedding, G.R.; McArthur, J. Span Efficiencies of Wings at Low Reynolds Numbers. *J. Aircr.* **2010**, *47*, 120–128. [[CrossRef](#)]
27. Montejano, M.A.B.; Sevillano, A.R.; Rojo, M.E.R.; Morales-Serrano, S. A wind tunnel two-dimensional parametric investigation of biplane configurations. *J. Mech. Eng. Autom.* **2014**, *4*, 412–421. Available online: <http://oa.upm.es/34874/> (accessed on 7 March 2022).
28. Frediani, A. The Prandtl Wing. *VKI Lect. Ser. Innov. Config. Adv. Concepts Futur. Civ. Aircr.* **2005**, 1–23.
29. Frediani, A.; Gasperini, M.; Saporito, G.; Rimondi, A. Development of a Prandtl Plane aircraft configuration. *Proc. Inst. Mech. Eng. Part I J. Syst. Control. Eng.* **2003**, *222*, 2263–2276.
30. Luciano, D.; Antonio, D.; Giovanni, M.; Rauno, C. An Invariant Formulation for the Minimum Induced Drag Conditions of Non-planar Wing Systems. In Proceedings of the 52nd Aerospace Sciences Meeting, National Harbor, ML, USA, 13–17 January 2014; pp. 13–17.
31. Pelletier, A.; Mueller, T.J. Low Reynolds number aerodynamics of low-aspect-ratio, thin/flat/cambered-plate wings. *J. Aircr.* **2000**, *37*, 825–832. [[CrossRef](#)]
32. Jones, R.; Cleaver, D.J.; Gursul, I. Aerodynamics of biplane and tandem wings at low Reynolds numbers. *Exp. Fluids* **2015**, *56*, 1047–1062. [[CrossRef](#)]
33. Selig, M.S.; Guglielmo, J.J. High-lift low Reynolds number airfoil design. *J. Aircr.* **1997**, *34*, 72–79. [[CrossRef](#)]
34. Owen, F.K.; Owen, A.K. Measurement and assessment of wind tunnel flow quality. *Prog. Aerosp. Sci.* **2008**, *44*, 315–348. [[CrossRef](#)]
35. Mueller, T.J.; DeLaurier, J.D. Aerodynamics of small vehicles. *Annu. Rev. Fluid Mech.* **2003**, *35*, 89–111. [[CrossRef](#)]
36. Mueller, T.J. On the birth of micro air vehicles. *Int. J. Micro Air Veh.* **2009**, *1*, 1–12. [[CrossRef](#)]